Computer Assisted Mechanics and Engineering Sciences, 9: 341–357, 2002.

Non-linear dynamics of flexible shell structures[1]

Jacek Chróścielewski
Technical University of Gdańsk, Division of Bridges
ul. Narutowicza 11/12, 80-952 Gdańsk, Poland

Jerzy Makowski
Ruhr University of Bochum, Lehrstuhl für Allgemeine Mechanik
Universitätstr. 150 IA3, D 44780 Bochum, Germany

Wojciech Pietraszkiewicz
Polish Academy of Sciences, Institute of Fluid-Flow Machinery
ul. Gen. J. Fiszera, 80-952 Gdańsk, Poland

(Received August 8, 2000)

The initial-boundary value problem in the weak form is formulated for the general six-field non-linear theory of branched shell structures. The extended time-stepping algorithm of the Newmark type is worked out for the non-linear dynamic analysis on the configuration space containing the rotation group $SO(3)$. Within the finite element approximation, an accurate indirect C^0 interpolation procedure on $SO(3)$ with a transport of approximation domain is developed. Numerical simulations by the finite element method of 2D and 3D large overall motions of several flexible elastic shell structures are presented. It is shown that values of potential and kinetic energies may oscillate in time, but the total energy remains conserved during the free motion of the structures in space.

1. Introduction

Dynamic behaviour of flexible shell structures undergoing finite deformations and large overall motion has recently gained a considerable interest. We refer to Simo, Rifai and Fox [16], Simo and Tarnow [17], Kuhl and Ramm [9], Madenci and Barut [12] and Brank, Briseghella, Tonello and Damjanic [1], where references to other papers are given.

The complete set of field equations as well as initial, boundary and continuity conditions describing an arbitrary motion of irregular shell structures containing folds, branches and/or self-intersections was derived in [3, 5, 6, 10, 15]. The 3D shell is represented by the 2D reference network consisting of a finite number of surface elements joined together along parts of their boundaries. Contrary to a variety of shell models discussed in the literature, the 2D balance laws of shell dynamics are given here in terms of through-the-thickness resultant quantities as exact implications of basic laws of 3D continuum mechanics. The shell evolution in time is described by two fields defined over the network: the vector field $\boldsymbol{u}$ representing the translatory motion of the reference network, and the proper orthogonal tensor field $\boldsymbol{Q}$ representing the mean rotary motion of the shell cross sections. The weak formulation of dynamics of the irregular shell structures based on this shell model is summarised in Section 2.

The aim of this report is to develop for this six-field shell model a time-stepping algorithm for transient dynamic analysis, and to perform some numerical simulations of the behaviour of regular

[1]This is an extended version of the article presented at the NATO Advanced Research Workshop on the *Computational Aspects of Nonlinear Structural Systems with Large Rigid Body Motion*, Pułtusk, Poland, July 2–7, 2000.

shells as well as branched, elastic shell structures in forced and free large overall motion.

There are many time-stepping schemes proposed in the literature, where stability and accuracy are most discussed properties of the algorithms. Among recent papers in the non-linear structural dynamics, we refer to Kuhl and Crisfield [8] who discussed several time-stepping algorithms with the properties of numerical dissipation, enforced conservation of energy, algorithmic conservation of energy and combined ones. Similar discussion within the non-linear shell dynamics was given, among others, in Kuhl and Ramm [9]. In our shell model one of the two main independent field variables, $\boldsymbol{Q} \in SO(3)$, is an element of the non-linear manifold but not a linear space. As a result, standard time-stepping integrators used in non-linear structural dynamics cannot be directly applied.

The numerical time stepping algorithm developed here, in part dealing with the orthogonal group, is based on ideas suggested, among others, by Simo and Vu-Quoc [18], Cardona and Geradin [2], Simo and Wong [19] and Simo and Tarnow [17]. In particular, we take into account that: a) the Newmark integration scheme assures the best possible convergence and stability; b) external loads are well defined only in the spatial representation; c) angular velocity and acceleration vectors at different time steps can be added directly only in the material representation; d) one should try to conserve the total energy of the system in incremental force-free motion. We use our experience in shell statics [3, 5, 6] and propose in the iterative process an exact calculation scheme of the incremental, relative rotation vector. The material representation of this vector plays a crucial role in the time-stepping algorithm.

For spatial discretisation the finite element method is applied. In order to increase the interpolation accuracy for $SO(3)$-valued fields, we have worked out an accurate, indirect interpolation procedure with a transport of approximation domain into the neighbourhood of the neutral element $\mathbf{1} \in SO(3)$. Within each finite element the procedure practically removes any singularity following from a local parameterisation, and does not impose any particular parameterisation of $\boldsymbol{Q}$. This type of interpolation is of particular importance in dynamic problems of flexible shell structures undergoing large overall motion discussed here. In these problems both the translations and rotations are not bounded at all.

Within the numerical analysis we perform several dynamic simulations of the 2D and 3D large overall motion of flexible, regular and branched, elastic shell structures the results of which are given in Section 6.

2. Weak formulation of non-linear dynamics of irregular shells

Within the general theory of irregular shell structures, the initial (undeformed) configuration of the 3D shell-like body is represented by a 2D surface-like continuum M called briefly an (undeformed) reference network [6, 13]. The network consists of a finite number of regular surface elements $M^{(k)}$, $k = 1, 2, \ldots, K$, joined together along parts of their boundaries $\partial M^{(k)}$. Each $M^{(k)}$ is a bounded, oriented, connected and smooth surface whose boundaries $\partial M^{(k)}$ consist of a finite number of closed, piecewise smooth curves. Common parts of boundaries of any two or more distinct surface elements form a spatial curve, and a union of all such curves is called briefly a singular curve $\Gamma \subset M$. Therefore, we have the following definitions,

$$M = \bigcup_{k=1}^{K} \left(M^{(k)} \cup \partial M^{(k)} \right), \qquad \Gamma = \bigcup_{\substack{m,n=1 \\ m \neq n}}^{K} \partial M^{(m)} \cap \partial M^{(n)}, \qquad \partial M = \left(\bigcup_{k=1}^{K} \partial M^{(k)} \right) \backslash \Gamma. \tag{1}$$

With each regular point $\boldsymbol{x} \in M$ we can associate the position vector $\boldsymbol{x} \in E^3$ relative to an inertial frame $(o, \mathbf{e}_i)$, where $o \in \mathcal{E}^3$ is a point of the 3D Euclidean point space and $\mathbf{e}_i \in E^3$, $i = 1, 2, 3$, are orthonormal vectors. If (ξ^α), $\alpha = 1, 2$, are surface co-ordinates, with each regular $\boldsymbol{x} \in M$ we can associate the natural surface base vectors and the unit normal vector defined by

$$\boldsymbol{a}_\alpha = \frac{\partial \boldsymbol{x}}{\partial \xi^\alpha} \equiv \boldsymbol{x}_{,\alpha}, \qquad \boldsymbol{a}^\beta \cdot \boldsymbol{a}_\alpha = \delta_\alpha^\beta, \qquad \boldsymbol{a}_3 = \frac{1}{2} \epsilon^{\alpha\beta} \boldsymbol{a}_\alpha \times \boldsymbol{a}_\beta, \tag{2}$$

where $\epsilon^{\alpha\beta}$ are surface permutation symbols.

The motion of the shell in time t can be described by two fields defined over the reference network: the position vector field $\boldsymbol{y}(\boldsymbol{x},t)$ representing the translatory motion of the shell reference network, and the proper orthogonal tensor field $\boldsymbol{Q}(\boldsymbol{x},t)$ representing the mean rotary motion of the shell cross sections.

The general mechanical theory of irregular shell structures was developed in [3, 6]. Within this approach the 2D resultant balance equations of translational and rotational momenta as well as the dynamical boundary and continuity conditions are exact implications of the balance laws of 3D continuum mechanics. The 2D kinematic structure of the shell consisting of the appropriate independent kinematic fields, the kinematic relations, as well as the kinematic boundary, continuity and initial conditions is then constructed again exactly from the 2D virtual work identity. Unavoidable approximations enter the shell theory only through kinetic and material constitutive relations. We refer the reader to papers mentioned above as well as to Chróścielewski, Makowski and Stumpf [5] and Libai and Simmonds [10] for details of the derivation process, necessary regularity assumptions for all the fields and references to other papers.

In this report we confine ourselves only to geometric irregularities and allow the shell to have only folds, branches and/or self-intersections. We assume from the beginning that the kinematic fields $\boldsymbol{y}(\boldsymbol{x},t)$ and $\boldsymbol{Q}(\boldsymbol{x},t)$ are continuous during the motion, and $\boldsymbol{y}_\Gamma(\boldsymbol{x}_\Gamma\,,\,t) = \boldsymbol{y}(\boldsymbol{x},t)|_\Gamma$, $\boldsymbol{Q}_\Gamma(\boldsymbol{x}_\Gamma\,,\,t) = \boldsymbol{Q}(\boldsymbol{x},t)|_\Gamma$, with $\boldsymbol{x}_\Gamma \in \Gamma$. We do not associate here any mechanical properties with the singular curve Γ as well.

When expressed in the weak form, the initial-boundary value problem (IBVP) for the irregular shell-like structure can be formulated as follows: Given the external resultant force and couple vector fields $\boldsymbol{f}(\boldsymbol{x},t)$ and $\boldsymbol{c}(\boldsymbol{x},t)$ on $\boldsymbol{x} \in M\backslash\Gamma$, $\boldsymbol{n}^*(\boldsymbol{x},t)$ and $\boldsymbol{m}^*(\boldsymbol{x},t)$ along ∂M_f, $\boldsymbol{f}_\Gamma(\boldsymbol{x},t)$ and $\boldsymbol{c}_\Gamma(\boldsymbol{x},t)$ along the singular curve $\Gamma \subset M$, and the initial values $\boldsymbol{u}_0(\boldsymbol{x})$, $\boldsymbol{Q}_0(\boldsymbol{x})$, $\dot{\boldsymbol{u}}_0(\boldsymbol{x})$, $\dot{\boldsymbol{Q}}_0(\boldsymbol{x})$ at $t = 0$, find a curve $\mathbb{u}(\boldsymbol{x},t) = (\,\boldsymbol{u}(\boldsymbol{x},t)\,,\,\boldsymbol{Q}(\boldsymbol{x},t)\,)$ on the configuration space $C(M\,,\,E^3 \times SO(3))$ such that for any continuous, kinematically admissible virtual vector fields $\mathbb{w}(\boldsymbol{x}) \equiv (\boldsymbol{v}(\boldsymbol{x}), \boldsymbol{w}(\boldsymbol{x})) \in V_A(M\,,\,E^3 \times E^3)$ we have

$$
\begin{aligned}
G[\mathbb{u},t;\mathbb{w}] = {} & \iint_{M\backslash\Gamma} [\dot{\boldsymbol{p}} \cdot \boldsymbol{v} + (\dot{\boldsymbol{m}} + \boldsymbol{v} \times \boldsymbol{p}) \cdot \boldsymbol{w}]\, \mathrm{d}a + \iint_{M\backslash\Gamma} \left[\boldsymbol{n}^\beta \cdot (\boldsymbol{v}_{,\beta} + \boldsymbol{y}_{,\beta} \times \boldsymbol{w}) + \boldsymbol{m}^\beta \cdot \boldsymbol{w}_{,\beta}\right] \mathrm{d}a \\
& - \iint_{M\backslash\Gamma} (\boldsymbol{f} \cdot \boldsymbol{v} + \boldsymbol{c} \cdot \boldsymbol{w})\, \mathrm{d}a - \int_{\partial M_f} (\boldsymbol{n}^* \cdot \boldsymbol{v} + \boldsymbol{m}^* \cdot \boldsymbol{w})\, \mathrm{d}s \\
& - \int_\Gamma (\boldsymbol{f}_\Gamma \cdot \boldsymbol{v}_\Gamma + \boldsymbol{c}_\Gamma \cdot \boldsymbol{w}_\Gamma)\, \mathrm{d}s = 0.
\end{aligned} \tag{3}
$$

Here, $\boldsymbol{v}(\boldsymbol{x},t) = \dot{\boldsymbol{y}}(\boldsymbol{x},t) = \dot{\boldsymbol{u}}(\boldsymbol{x},t)$ is the network velocity vector, $\boldsymbol{u}(\boldsymbol{x},t) = \boldsymbol{y}(\boldsymbol{x},t) - \boldsymbol{x}$ is the network displacement vector, $\boldsymbol{p}(\boldsymbol{x},t)$ and $\boldsymbol{m}(\boldsymbol{x},t)$ are the translational and rotational momenta vectors, $\boldsymbol{n}^\beta(\boldsymbol{x},t)$ and $\boldsymbol{m}^\beta(\boldsymbol{x},t)$ are the internal stress and couple resultant vectors, respectively, and $\boldsymbol{v}_\Gamma = \boldsymbol{v}|_\Gamma$, $\boldsymbol{w}_\Gamma = \boldsymbol{w}|_\Gamma$. In Eq. (3) it is implicitly assumed that the kinematic boundary conditions $\boldsymbol{u}(\boldsymbol{x},t) = \boldsymbol{u}^*(\boldsymbol{x},t)$ and $\boldsymbol{Q}(\boldsymbol{x},t) = \boldsymbol{Q}^*(\boldsymbol{x},t)$ are satisfied on the complementary part $\partial M_d = \partial M\backslash\partial M_f$, and the virtual vector fields are kinematically admissible if $\boldsymbol{v}(\boldsymbol{x}) = \boldsymbol{0}$ and $\boldsymbol{w}(\boldsymbol{x}) = \boldsymbol{0}$ on ∂M_d.

In the shell theory the explicit expressions for the momenta $\boldsymbol{p}$ and $\boldsymbol{m}$ should be specified by the kinetic constitutive relations, in general. In this report we shall use simple relations suggested by Simmonds [15],

$$
\boldsymbol{p} = m_0 \boldsymbol{v} = \rho_0 h_0 \boldsymbol{v}, \qquad \boldsymbol{m} = I_0 \boldsymbol{\omega} = \frac{\rho_0 h_0^3}{12}\, \boldsymbol{\omega}, \qquad \boldsymbol{\omega} \times \boldsymbol{1} = \dot{\boldsymbol{Q}} \boldsymbol{Q}^T, \tag{4}
$$

where $\rho_0(\boldsymbol{x})$ is the initial mass density, $h_0(\boldsymbol{x})$ is the initial shell thickness, and $\boldsymbol{\omega}(\boldsymbol{x},t)$ is the network spin vector in the spatial representation.

The resultants $\boldsymbol{n}^{\beta}$ and $\boldsymbol{m}^{\beta}$ should be given through the constitutive relations of the material the shell is composed of. In this report we restrict our interest to the hyper-elastic shells for which there exists a 2D strain energy function $\mathcal{W}(\boldsymbol{\varepsilon}_{\beta}, \boldsymbol{\kappa}_{\beta}; \boldsymbol{x})$ of the shell strain vectors which are defined by

$$\boldsymbol{\varepsilon}_{\beta} = \boldsymbol{y}_{,\beta} - \boldsymbol{Q}\boldsymbol{a}_{\beta}, \qquad \boldsymbol{\kappa}_{\beta} \times \mathbf{1} = \boldsymbol{Q}_{,\beta}\boldsymbol{Q}^{T}. \tag{5}$$

Then the constitutive relations of the shell material are given by

$$\boldsymbol{n}^{\beta} = \frac{\partial \mathcal{W}}{\partial \boldsymbol{\varepsilon}_{\beta}}, \qquad \boldsymbol{m}^{\beta} = \frac{\partial \mathcal{W}}{\partial \boldsymbol{\kappa}_{\beta}}. \tag{6}$$

The solution of the non-linear IBVP (3) is achieved by an incremental-iterative procedure which reduces the problem to a sequence of solutions of linearised problems. Each linearised problem is formulated at discrete values of both temporal and spatial variables. The main difficulty of the solution procedure is associated with the structure of the configuration space $C(M, E^3 \times SO(3))$ involving the proper orthogonal group $SO(3)$. As a result, the solution procedure requires special techniques for approximation, parameterisation, interpolation, and accumulation of the $SO(3)$-valued fields.

3. Extended Newmark time-stepping algorithm

Let the time interval $[0, T]$ be partitioned by a finite number of time instants $0 \equiv t_0 < t_1 < \cdots < t_n < t_{n+1} < \cdots < t_N \equiv T$ such that $[0, T] = \bigcup_{n=0}^{N} [t_n, t_{n+1}]$ with $\Delta t = t_{n+1} - t_n$ a typical time step. Then, in general, the weak form of the IBVP at the time instant t_{n+1} can be written as

$$G_{n+1} \equiv G[\mathbb{u}_{n+1}, t_{n+1}; \mathbb{w}_{n+1}] = 0 \qquad \forall \mathbb{w}_{n+1} \in V_A, \tag{7}$$

for the unknown generalised displacement $\mathbb{u}_{n+1} \simeq \mathbb{u}(t_{n+1}) \in C$.

When integrating linear systems of dynamic equations the main attention is paid to the order of accuracy of integration schemes, for the criterion of unconditional stability of the scheme can easily be satisfied. In the non-linear computational dynamics the main interest is focused on numerical stability of time integrators. It is known that unconditionally stable algorithms of linear dynamics often lose this property in problems of non-linear dynamics. In the latter case a sufficient condition for some kind of numerical stability of the scheme is the conservation or decay of the total energy within a time step.

The energetic criterion for numerical stability can be written in the form

$$U_{n+1} - U_n + K_{n+1} - K_n \leq \Delta G_{\text{ext}}, \tag{8}$$

where $U_{n+1} \simeq U(t_{n+1})$ and $U_n \simeq U(t_n)$ are numerically calculated strain energies $U(t)$ at the beginning t_n and the end t_{n+1} of the time step Δt, K_{n+1} and K_n are the respective kinetic energies $K(t)$, while ΔG_{ext} represents the work done by external loads during the time step. It may happen, however, that the algorithm satisfying Eq. (8) can reach a solution point beyond which further advances in time integration by an incremental-iterative procedure are not possible.

Taking into account Eqs. (6), (4) and (3), terms in Eq. (8) have the following meaning:

$$\begin{aligned}
U &= \iint_{M\setminus\Gamma} \mathcal{W}\, \mathrm{d}a, \\
K &= \frac{1}{2} \iint_{M\setminus\Gamma} (m_0 \boldsymbol{v}\cdot\boldsymbol{v} + I_0 \boldsymbol{\omega}\cdot\boldsymbol{\omega})\, \mathrm{d}a, \\
\Delta G_{ext} &= \int_{t_n}^{t_{n+1}} \left\{ \iint_{M\setminus\Gamma} (\boldsymbol{f}\cdot\boldsymbol{v} + \boldsymbol{c}\cdot\boldsymbol{\omega})\, \mathrm{d}a \right. \\
&\qquad \left. + \int_{\partial M_f} (\boldsymbol{n}^{*}\cdot\boldsymbol{v} + \boldsymbol{m}^{*}\cdot\boldsymbol{\omega})\, \mathrm{d}s + \int_{\Gamma} (\boldsymbol{f}_{\Gamma}\cdot\boldsymbol{v}_{\Gamma} + \boldsymbol{c}_{\Gamma}\cdot\boldsymbol{\omega}_{\Gamma})\, \mathrm{d}s \right\} \mathrm{d}t,
\end{aligned} \tag{9}$$

where $\boldsymbol{v}_\Gamma(\boldsymbol{x}_\Gamma, t) = \boldsymbol{v}(\boldsymbol{x}, t)|_\Gamma$, $\boldsymbol{\omega}_\Gamma(\boldsymbol{x}_\Gamma, t) = \boldsymbol{\omega}(\boldsymbol{x}, t)|_\Gamma$.

There are many time-stepping algorithms proposed in the literature for solving dynamic problems in the linear space. Among engineers the most popular are those based on the implicit one-step Newmark [14] formula with the Newton iterations, in which the actual state at time t_{n+1} is calculated from the former state at time t_n alone. In case of the non-linear shell dynamics discussed here the configuration space C does not have the structure of the linear space. In this case essential difficulties arise in the extension of classical time-stepping algorithms to hold in C. Several extensions of the Newmark formula to the rotation group $SO(3)$ were proposed in [2, 17–19]. In the extensions concepts of differential geometry such as exponential map and parallel transport play the important role.

In the proposed time-stepping algorithm described below we also extend to the rotation group $SO(3)$ the Newmark formula, but in the algorithm on $SO(3)$ the following properties of some fields have explicitly been used:

1. The physical meaning of external loads is well defined only in the spatial representation. Thus, the generalised momentum balance is formulated in the spatial representation as well. The linearised dynamic equations are written relative to an instantaneous configuration $\mathbb{u}_{n+1}^{(i)}$, that is at the i-th approximation to $\mathbb{u}_{n+1} = \mathbb{u}(t_{n+1})$, and not relative to $\mathbb{u}_n$. This eliminates the need of applying the transformation relation of the type

$$\boldsymbol{Y}_n(\boldsymbol{Q}_{n+1}^{(i)}) \; : \; T_{\boldsymbol{Q}_{n+1}^{(i)}} SO(3) \to T_{\boldsymbol{Q}_n} SO(3)$$

appearing in [2, 18], for in our case $\boldsymbol{Y} \equiv \mathbf{1}$.

2. Angular velocities and accelerations from different time instants can directly be added only in material representation [19]. Therefore, temporal approximations of these fields are performed in the material representation, then results are transformed into the spatial representation and introduced into the linearised dynamic equations.

Let us remind that the time change of the rotation field $\boldsymbol{Q} \in SO(3)$,

$$\dot{\boldsymbol{Q}} = \boldsymbol{\Omega}\boldsymbol{Q} = \boldsymbol{Q}\boldsymbol{\Omega}, \tag{10}$$

allows one to introduce angular velocities and accelerations either in the spatial representation

$$\boldsymbol{\Omega} = \dot{\boldsymbol{Q}}\boldsymbol{Q}^T = \boldsymbol{\omega} \times \mathbf{1}, \qquad \boldsymbol{A} = \dot{\boldsymbol{\Omega}} = \ddot{\boldsymbol{Q}}\boldsymbol{Q}^T - \boldsymbol{\Omega}\boldsymbol{\Omega} = \boldsymbol{a} \times \mathbf{1}, \tag{11}$$

or in the material representation

$$\boldsymbol{\Omega} = \boldsymbol{Q}^T\dot{\boldsymbol{Q}} = \boldsymbol{\omega} \times \mathbf{1}, \qquad \mathsf{A} = \dot{\boldsymbol{\Omega}} = \boldsymbol{Q}^T\ddot{\boldsymbol{Q}} - \boldsymbol{\Omega}\boldsymbol{\Omega} = \mathsf{a} \times \mathbf{1}. \tag{12}$$

Both representations are related by

$$\boldsymbol{\Omega} = \boldsymbol{Q}\boldsymbol{\Omega}\boldsymbol{Q}^T, \qquad \boldsymbol{\omega} = \boldsymbol{Q}\boldsymbol{\omega}, \qquad \boldsymbol{A} = \boldsymbol{Q}\mathsf{A}\boldsymbol{Q}^T, \qquad \boldsymbol{a} = \boldsymbol{Q}\mathsf{a}. \tag{13}$$

The generalised displacements $\mathbb{u}_n$, velocities $\mathbb{v}_n$, and accelerations $\mathbb{a}_n$ numerically calculated at the time instant t_n are denoted by

$$\begin{aligned} \mathbb{u}_n &= (\boldsymbol{u}_n, \boldsymbol{Q}_n) \simeq (\boldsymbol{u}(t_n), \boldsymbol{Q}(t_n)), \\ \mathbb{v}_n &= (\dot{\boldsymbol{u}}_n, \boldsymbol{\omega}_n) \simeq (\dot{\boldsymbol{u}}(t_n), \boldsymbol{\omega}(t_n)), \\ \mathbb{a}_n &= (\ddot{\boldsymbol{u}}_n, \mathsf{a}_n) \simeq (\ddot{\boldsymbol{u}}(t_n), \mathsf{a}(t_n)). \end{aligned} \tag{14}$$

The basic problem of our time-stepping algorithm can be formulated as follows: Given $\mathbb{u}_n$, $\mathbb{v}_n$, $\mathbb{a}_n$ at the time instant t_n, find $\mathbb{u}_{n+1}$, $\mathbb{v}_{n+1}$, $\mathbb{a}_{n+1}$ at the next time instant $t_{n+1} = t_n + \Delta t$ in the

way which is compatible with the problem equations (3) and numerically stable, e.g. in the sense of Eq. (8).

In the iterative solution of the linearised problem equations we assume to know the i-th correction of the incremental generalised displacements $\delta\mathbb{w}_{n+1}^{(i+1)} = (\delta\boldsymbol{u}_{n+1}^{(i+1)}, \delta\boldsymbol{w}_{n+1}^{(i+1)})$. Here $\delta\boldsymbol{w}_{n+1}^{(i+1)}$ ($\delta\boldsymbol{w} \times \mathbf{1} = \delta\boldsymbol{W} = \delta\boldsymbol{Q}\boldsymbol{Q}^T$) is the i-th correction of the incremental rotation vector in the spatial representation. Since the part of algorithm associated with the translatory motion $(\boldsymbol{u}, \dot{\boldsymbol{u}}, \ddot{\boldsymbol{u}})$ is standard, we present below only the main steps associated with the rotational part $(\boldsymbol{Q}, \boldsymbol{\omega}, \mathbf{a})$ of the algorithm. These steps are:

1. Update the rotation tensor in the spatial representation

$$\boldsymbol{Q}_{n+1}^{(i+1)} = \exp\left(\delta\boldsymbol{W}_{n+1}^{(i+1)}\right)\boldsymbol{Q}_{n+1}^{(i)}, \qquad \delta\boldsymbol{W}_{n+1}^{(i+1)} = \delta\boldsymbol{w}_{n+1}^{(i+1)} \times \mathbf{1}, \qquad i = 0, 1, 2, 3, \ldots, \tag{15}$$

$$\boldsymbol{Q}_{n+1}^{(0)} \equiv \boldsymbol{Q}_n, \qquad \delta\boldsymbol{w}_{n+1}^{(1)} \equiv \Delta\boldsymbol{w}_n^{(1)}.$$

2. Calculate the complete increment of the rotation vector $\Delta\mathbf{w}_n^{(i+1)}$ in the material representation

$$\exp\left(\Delta\mathbf{W}_n^{(i+1)}\right) = \boldsymbol{Q}_n^{\mathrm{T}}\boldsymbol{Q}_{n+1}^{(i+1)}, \qquad \Delta\mathbf{W}_n^{(i+1)} = \Delta\mathbf{w}_n^{(i+1)} \times \mathbf{1}. \tag{16}$$

3. Calculate angular accelerations and velocities in the material representation according to the extended Newmark scheme

$$\begin{aligned} \mathbf{a}_{n+1}^{(i+1)} &= \frac{1}{\beta(\Delta t)^2}\left[\Delta\mathbf{w}_n^{(i+1)} - \Delta t\,\boldsymbol{\omega}_n - (\Delta t)^2\left(\frac{1}{2} - \beta\right)\mathbf{a}_n\right], \\ \boldsymbol{\omega}_{n+1}^{(i+1)} &= \frac{\gamma}{\beta\Delta t}\Delta\mathbf{w}_n^{(i+1)} + \left(1 - \frac{\gamma}{\beta}\right)\boldsymbol{\omega}_n + \Delta t\left(1 - \frac{\gamma}{2\beta}\right)\mathbf{a}_n. \end{aligned} \tag{17}$$

4. Transform the vectors (17) to the spatial representation

$$\boldsymbol{\omega}_{n+1}^{(i+1)} = \boldsymbol{Q}_{n+1}^{(i+1)}\boldsymbol{\omega}_{n+1}^{(i+1)}, \qquad \boldsymbol{a}_{n+1}^{(i+1)} = \boldsymbol{Q}_{n+1}^{(i+1)}\mathbf{a}_{n+1}^{(i+1)}. \tag{18}$$

5. Formulate the problem linearised equations at the new iteration step $i \to i+1$ and calculate the new correction of $\delta\boldsymbol{w}$.

The parameters $0 \leq \beta \leq 0.5$ and $0 \leq \gamma \leq 1$ in Eq. (17) are free parameters of the Newmark algorithm. Specialisation of β and γ leads to a variety of time integration schemes known in E^3 and to various their extensions into $E^3 \times SO(3)$.

4. Iterative solution of the non-linear problem

With the time-stepping algorithm developed in Section 3, the solution of the non-linear problem (7) is constructed by the incremental-iterative procedure based on the Newton–Kantorovich method [7] applied in the configuration space $C(M, E^3 \times SO(3))$. Let an i-th approximation $\mathbb{w}_{n+1}^{(i)}$ to the solution $\mathbb{w}_{n+1}$ has been found. In order to calculate the correction $\delta\mathbb{w}_{n+1}^{(i+1)}$, which would allow us to find the successive approximation $\mathbb{w}_{n+1}^{(i+1)}$ to the unknown solution $\mathbb{w}_{n+1}$, we linearise Eq. (7) at the approximation $\mathbb{w}_{n+1}^{(i)}$,

$$G\left[\mathbb{w}_{n+1}^{(i)}, t_{n+1}; \mathbb{w}\right] + \delta G\left[\mathbb{w}_{n+1}^{(i)}, t_{n+1}; \mathbb{w}, \delta\mathbb{w}_{n+1}^{(i+1)}\right] = 0. \tag{19}$$

The second term in Eq. (19) denotes a directional derivative of the functional (7), taken at the point $\mathbb{w}_{n+1}^{(i)} \in C$ in the direction $\delta\mathbb{w}_{n+1}^{(i+1)} \in T_{\mathbb{w}_{n+1}^{(i)}} C$. This term yields the so-called tangent operator of the non-linear problem, calculated at the approximation $\mathbb{w}_{n+1}^{(i)}$. The first term in Eq. (19) represents unbalanced forces at the approximation point $\mathbb{w}_{n+1}^{(i)}$.

5. Spatial discretisation and interpolation in $SO(3)$

The main advantage of the mechanical theory of irregular shell structures discussed in Section 2 is that only C^0 continuity requirement is imposed upon the primary kinematic field $\mathbb{u}(\boldsymbol{u}, \boldsymbol{Q})$. When applying the finite element method we proceed as follows.

The shell reference network M (the domain) is divided into sub-domains $\Pi_{(e)}$, $e = 1, 2, \ldots, E$, (finite elements) such that $M = \bigcup_{e=1}^{E} \Pi_{(e)}$. A typical finite element $\Pi_{(e)}$ is a smooth image of a compact, bounded region $\pi_{(e)} \in R^2$, usually a triangle or a rectangle. Let $\boldsymbol{\eta} = (\eta_1, \eta_2)$ be local co-ordinates of $\pi_{(e)}$, $\Delta = \{\boldsymbol{\eta}_a \in \pi_{(e)}, a = 1, 2, \ldots, A\}$ be a set of A distinct points of $\pi_{(e)}$ called the nodes, $\mathbb{u}(\boldsymbol{\eta}) = (\boldsymbol{u}(\boldsymbol{\eta}), \boldsymbol{Q}(\boldsymbol{\eta})) \in C(\pi_{(e)}, E^3 \times SO(3))$ be a given smooth function on $\pi_{(e)}$ with values in the six-dimensional Lie group $E^3 \times SO(3)$, and let $\mathbb{u}_a = (\boldsymbol{u}_a, \boldsymbol{Q}_a) = (\boldsymbol{u}(\boldsymbol{\eta}_a), \boldsymbol{Q}(\boldsymbol{\eta}_a))$ denote values of $\mathbb{u}$ at the nodes $\boldsymbol{\eta}_a$. Within each $\pi_{(e)}$ we have to construct an approximating function $\tilde{\mathbb{u}}(\boldsymbol{\eta}) = (\tilde{\boldsymbol{u}}(\boldsymbol{\eta}), \tilde{\boldsymbol{Q}}(\boldsymbol{\eta}))$ which takes the same values at the nodes $\boldsymbol{\eta}_a$ as $\mathbb{u}$ does (that is $\tilde{\mathbb{u}}(\boldsymbol{\eta}_a) = \mathbb{u}_a$ for any $\boldsymbol{\eta}_a \in \Delta$) and is "close" – in some defined sense – to the given function $\mathbb{u}(\boldsymbol{\eta})$.

The standard C^0 interpolation at the nodes $\boldsymbol{\eta}_a$ of the E^3-valued function $\boldsymbol{u}(\boldsymbol{\eta})$ takes the form

$$\tilde{\boldsymbol{u}}(\boldsymbol{\eta}) = \sum_{a=1}^{A} N_a(\boldsymbol{\eta}) \boldsymbol{u}_a , \tag{20}$$

where $N_a(\boldsymbol{\eta})$ are given shape functions (usually products of the Lagrange polynomials, see Zienkiewicz [20]) satisfying the conditions $N_a(\boldsymbol{\eta}_b) = \delta_{ab}$ for any $\boldsymbol{\eta}_b \in \Delta$.

For the $SO(3)$-valued function such a standard, canonical interpolation scheme is not available. We proposed in [5] a kind of indirect C^0 interpolation procedure on $SO(3)$ through interpolation of three scalar functions $\vartheta_k(\boldsymbol{\eta})$ of local parameters. Numerical test examples presented in [4] indicate, however, that the procedure leads to a decrease of interpolation accuracy away from the neutral element $\mathbf{1} \in SO(3)$. Here we propose a modified, free from such a defect, indirect C^0 interpolation procedure on $SO(3)$ with a transport of approximation domain into the neighbourhood of the neutral element $\mathbf{1} \in SO(3)$ (see also [3]).

Let a local parameterisation of the rotation group be given by

$$\boldsymbol{Q} \xrightarrow{\mathcal{Q}} (\vartheta_k), \tag{21}$$

where $\boldsymbol{Q} \in U \subset SO(3)$ and $(\vartheta_k) = \mathcal{Q}(\boldsymbol{Q}) \in V \subset R^3$, $k = 1, 2, 3$, are three chosen, independent local parameters, and $\boldsymbol{Q}(\boldsymbol{\eta}) = \mathcal{Q}^{-1}(\vartheta_k(\boldsymbol{\eta}))$. The modified interpolation procedure on $SO(3)$ consists of the following steps:

1. Establishing for the set of nodal tensors $\boldsymbol{Q}_a = \boldsymbol{Q}(\boldsymbol{\eta}_a) \in U \subset SO(3)$ a constant, averaged representative $\bar{\boldsymbol{Q}} \in SO(3)$.

2. Transporting the set $\boldsymbol{Q}_a$ by the kind of pull-back with $\bar{\boldsymbol{Q}}^T : U \to W \subset SO(3)$ into the "neighbourhood" of $\mathbf{1} \in W \subset SO(3)$,

$$\boldsymbol{R}_a = \bar{\boldsymbol{Q}}^T \boldsymbol{Q}_a . \tag{22}$$

3. Introducing three local parameters in the map $(W, \mathcal{R})$ for the transported tensor field,

$$(\rho_k)_a = \mathcal{R}(\boldsymbol{R}_a). \tag{23}$$

4. Interpolating the scalar functions $\rho_k(\boldsymbol{\eta}) \in R^3$ through the nodal values $(\rho_k)_a$ according to the scheme (20),

$$\tilde{\boldsymbol{\rho}}(\boldsymbol{\eta}) = \sum_{a=1}^{A} N_a(\boldsymbol{\eta}) \boldsymbol{\rho}_a . \tag{24}$$

5. Calculating the interpolating tensor function $\tilde{\boldsymbol{R}}(\boldsymbol{\eta})$,

$$\tilde{\boldsymbol{R}}(\boldsymbol{\eta}) = \mathcal{R}^{-1}(\tilde{\boldsymbol{\rho}}(\boldsymbol{\eta})). \tag{25}$$

6. Transporting back the function $\tilde{\boldsymbol{R}}(\boldsymbol{\eta})$ into the initial position in $SO(3)$ by the kind of push-forward with $\bar{\boldsymbol{Q}} : W \to U \subset SO(3)$,

$$\tilde{\boldsymbol{Q}}(\boldsymbol{\eta}) = \bar{\boldsymbol{Q}}\tilde{\boldsymbol{R}}(\boldsymbol{\eta}). \tag{26}$$

Therefore, $\tilde{\boldsymbol{Q}}(\boldsymbol{\eta})$ interpolates the given function $\boldsymbol{Q}(\boldsymbol{\eta}) \in C(\pi_{(e)}, SO(3))$ at the set of nodes $\boldsymbol{\eta}_a \in \Delta$ indeed. From Eq. (26) it also follows that the interpolating function $\tilde{\boldsymbol{Q}}(\boldsymbol{\eta})$ always takes values in the rotation group. Within each finite element the proposed interpolation procedure practically removes any singularity which may follow from a local parameterisation. The procedure itself does not impose any particular parameterisation of $\boldsymbol{Q}$. As a result, it can be used for any non-singular global parameterisation of the rotation group $SO(3)$.

In the incremental-iterative procedure described in Section 4 the corrections of the incremental rotation vector $\delta\boldsymbol{w}$ and the virtual rotation vector $\boldsymbol{w}$ play different roles than the field of rotation tensor $\boldsymbol{Q}$ itself. In the numerical procedure the fields $\delta\boldsymbol{w}$ and $\boldsymbol{w}$ appear as the "unknown" ones. If they are expressed through the respective incremental $\delta\vartheta_k$ and virtual ω_k local parameters, the C^0 interelement continuity requirement is transferred to the chosen parameterisation. The necessity to fulfil continuity of the local parameters restricts applicability of the algorithm to problems contained in only one local map $(U, \mathcal{R})$. For a curved shell structure, and for dynamic problems in particular, this decreases the interpolation accuracy as well [4].

The correction of the rotation tensor $\delta\boldsymbol{Q}$ at each regular $\boldsymbol{Q} \in C(\pi_{(e)}, SO(3))$ is an element of the tangent space $T_{\boldsymbol{Q}}C(\pi_{(e)}, SO(3)) \approx C(\pi_{(e)}, T_{\boldsymbol{Q}}SO(3))$, where $\approx$ indicates an isomorphism. We also have further isomorphisms of spaces $T_{\boldsymbol{Q}}C(\pi_{(e)}, SO(3)) \approx C(\pi_{(e)}, so(3))$ and their elements $\delta\boldsymbol{Q} \to \delta\boldsymbol{W} \to \delta\boldsymbol{w}$ where $\delta\boldsymbol{W} = \delta\boldsymbol{Q}\boldsymbol{Q}^T = \delta\boldsymbol{w} \times \mathbf{1}$ is the skew-symmetric tensor having $\delta\boldsymbol{w}$ as the axial vector.

The virtual rotation vector $\boldsymbol{w}$ (as well as $\delta\boldsymbol{w}$) can be represented through components either in the co-rotating $\boldsymbol{t}_i(t)$ or in the fixed, global $\mathbf{e}_i$ bases. If $\boldsymbol{t}_i(t) = \boldsymbol{T}(t)\mathbf{e}_i = T_{ij}(t)\mathbf{e}_j$, where $\boldsymbol{T} \in SO(3)$, then

$$\boldsymbol{w} = w_i\boldsymbol{t}_i = \bar{w}_j\mathbf{e}_j = \bar{w}_jT_{ij}\boldsymbol{t}_i\,, \tag{27}$$

where the corresponding components are related by $\bar{w}_i = T_{ij}\bar{w}_j$. With Eq. (27) we obtain the matrix form of the interpolation formula

$$\begin{Bmatrix} \tilde{w}_1(\boldsymbol{\eta}) \\ \tilde{w}_2(\boldsymbol{\eta}) \\ \tilde{w}_3(\boldsymbol{\eta}) \end{Bmatrix} = \mathbb{T}(\boldsymbol{\eta}) \sum_{a=1}^{A} N_a(\boldsymbol{\eta}) \begin{Bmatrix} \bar{w}_{1a} \\ \bar{w}_{2a} \\ \bar{w}_{3a} \end{Bmatrix}, \qquad \mathbb{T}(\boldsymbol{\eta}) : \begin{Bmatrix} \bar{w}_1(\boldsymbol{\eta}) \\ \bar{w}_2(\boldsymbol{\eta}) \\ \bar{w}_3(\boldsymbol{\eta}) \end{Bmatrix} \to \begin{Bmatrix} w_1(\boldsymbol{\eta}) \\ w_2(\boldsymbol{\eta}) \\ w_3(\boldsymbol{\eta}) \end{Bmatrix}. \tag{28}$$

Components of the nodal parameters $\bar{w}_{ia}$ are given in the global, fixed base $\mathbf{e}_i$ common to all the elements and the nodes. This allows one to describe easily the junctions of different branches $M^{(k)}$ of M. The components $\bar{w}_{ia}$ and w_{ia} can easily be expressed in terms of nodal displacements which provides an engineering interpretation to these components.

6. Numerical simulations

In order to illustrate the effectiveness of the time-stepping algorithm proposed in Section 3, several numerical simulations of dynamic behaviour of shell structures undergoing large overall motion have been performed. In the finite element discretisation of the structure we have used primarily the accurate displacement/rotation based 16-node Lagrange shell element with the full integration of the element matrices. The element denoted here as CAM*e*9 (FI) and CAM*e*16 (FI) are described in [3, 5]. The numerical results reported here are obtained with the version of the Newmark scheme, when $\beta = 0.25$ and $\eta = 0.5$ are used in Eq. (17).

6.1. Free–free flexible beam undergoing large overall motion

This problem was analysed in several papers on beam dynamics in 2D and 3D formulation, for example in [18] using the rod model. The beam initially at an inclined position in the plane ($\mathbf{e}_1$, $\mathbf{e}_3$) is loaded at the lower end by a spatially fixed force P and torque M with components and time histories as in Fig. 1. We solve here the same problem using the six-field shell model with the following data: $L = 10$, $L_x = 6$, $L_z = 8$, $L = (L_x^2 + L_z^2)^{1/2}$, $b = h_0 = 1$, $EA = 10^4$, $EJ = Ebh_0^3/12 = 500$, $\rho_0 A = 1$, $\rho_0 J = 10$. The beam is discretised by 1×10 *CAMe*16 (FI) and the time integration step is $\Delta t = 0.1$ sec. The deformation history of plane configurations of the beam is given in Fig. 2, while the sequence of plane configurations as seen from 3D perspective is shown in Fig. 1. Plots of energies depicted in Fig. 3 indicate small oscillations of the kinetic and potential energies, but the total energy remains constant in time. Our results confirm the dynamical behaviour of the rod discussed in other papers.

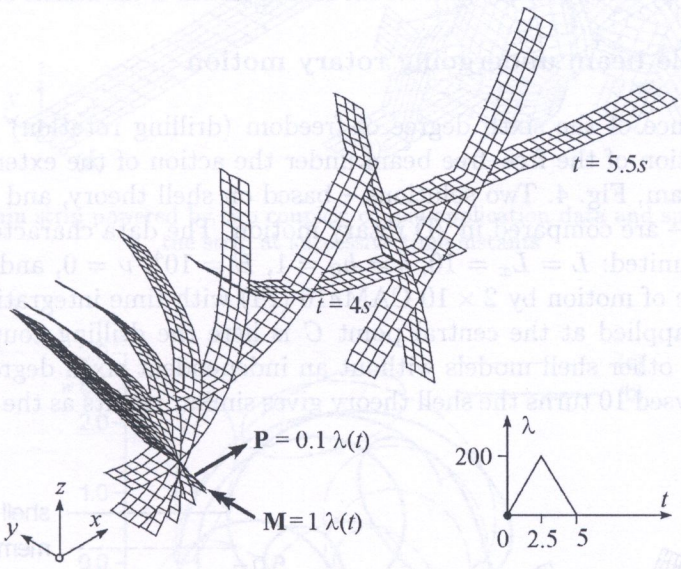

Fig. 1. 3D view of some configurations of the flexible beam in 2D free motion

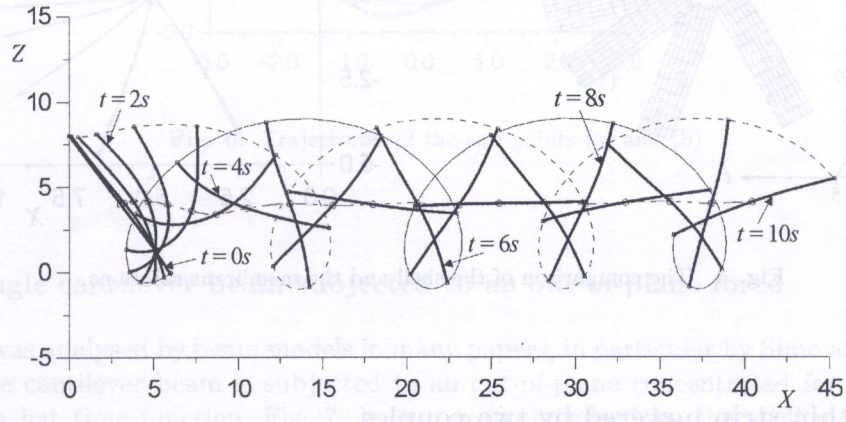

Fig. 2. Deformation history of the free–free flexible beam undergoing large overall 2D motion

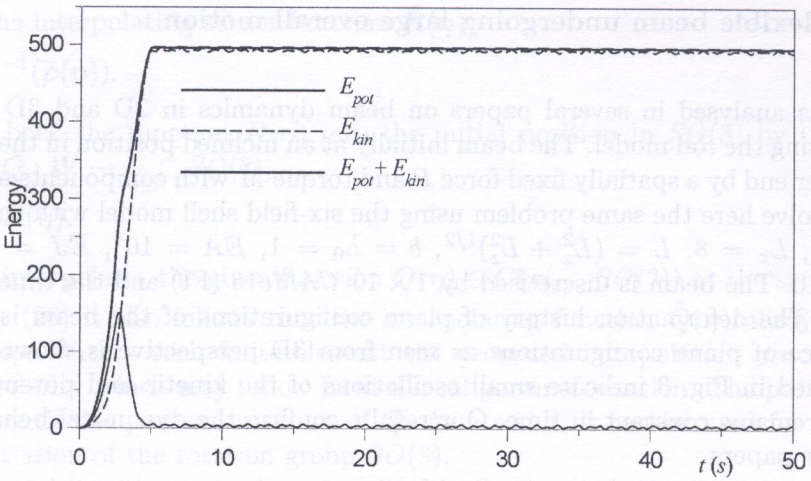

Fig. 3. Energy history plots for the 2D free motion of the flexible beam

6.2. Free–free flexible beam undergoing rotary motion

To verify the importance of the sixth degree of freedom (drilling rotation) in shell dynamics we analyse the rotary motion of the free–free beam under the action of the external couple applied at the centre C of the beam, Fig. 4. Two solutions – based on shell theory, and based on plane-stress elasticity (membrane) – are compared in 2D rotary motion. The data characteristics relative to the previous example are united: $L = L_x = 10$, $b = h_0 = 1$, $E = 10^4$, $\nu = 0$, and $\rho_0 = 1$. The beam is discretised in the plane of motion by 2×10 CAMe16 (FI) with time integration step $\Delta t = 0.1$ sec. Note that the couple applied at the central point C is here the drilling couple. Such an example cannot be analysed by other shell models without an independent sixth degree of freedom. In this example, over the analysed 10 turns the shell theory gives similar results as the plane-stress elasticity (membrane) solution.

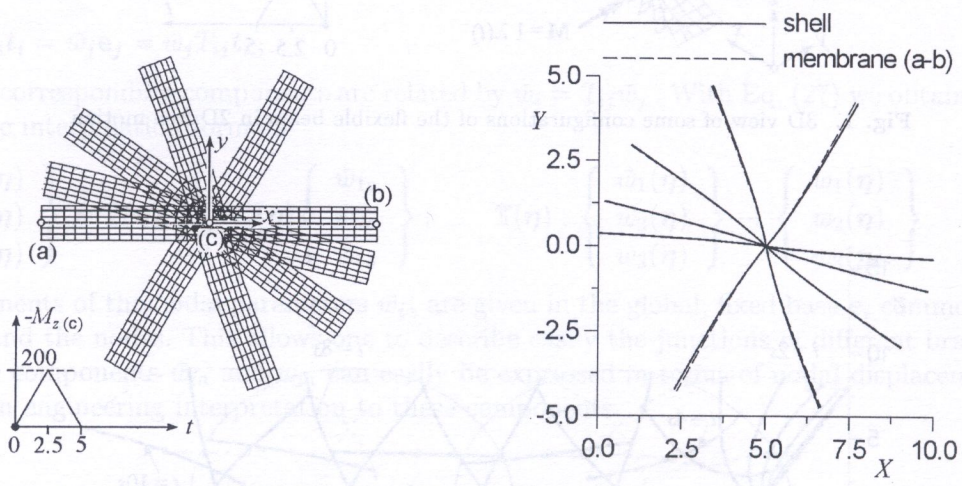

Fig. 4. The comparison of the shell and the membrane solutions

6.3. Free–free thin strip powered by two couples

By reducing 100 times the thickness of the beam from the previous example, we discuss the dynamic behaviour of the thin strip with data $L = L_x = 10$, $b = 1$, $h_0 = 0.01$, $E = 10^4$, $\nu = 0.25$, $\rho_0 = 1$.

The strip is powered by two dynamically applied couples: the couple $M_x(t)$ acting along the strip axis, and a small perturbing couple $M_y(t) = 0.05M_x(t)$, Fig. 5. The strip is discretised by 2×10 CAMe16 (FI) and the time integration step is $\Delta t = 0.005$ sec.

The problem illustrates the complex 3D motion of the strip developed from initial rotation about the X axis. Several spatial configurations at successive time instants are shown in Fig. 5, while Fig. 6 indicates the trajectories of the two end points (a) and (b) projected onto the X–Z co-ordinate plane. This example indicates large relative elastic deflections and multiple turns of some strip parts. In this problem the central point, where the couples are applied, should remain at the same spatial position through the simulation time. In our analysis it remains at the same position indeed. This can be regarded as an important control of correctness of the algorithm.

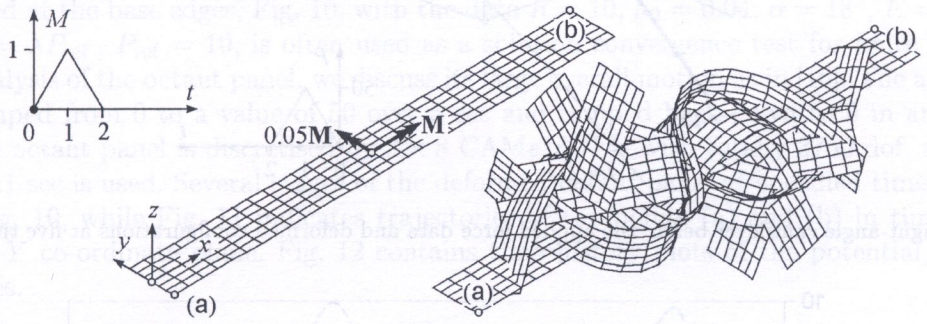

Fig. 5. Free–free thin strip powered by two couples: couple application data and spatial configurations of the strip at successive time instants

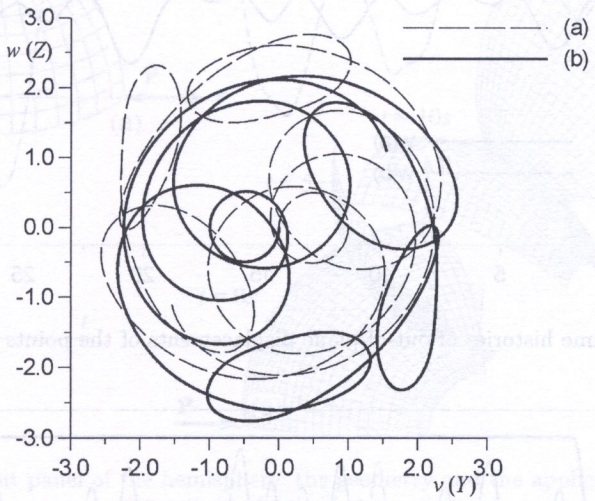

Fig. 6. Trajectories of the end points (a) and (b)

6.4. Right-angle cantilever beam subjected to an out-of-plane force

This problem was analysed by beam models in many papers, in particular by Simo and Vu-Quoc [18]. The right-angle cantilever beam is subjected to an out-of-plane concentrated force applied at the elbow (a) by a hat time function, Fig. 7. In our example solved by the shell model we take the data $L_x = L_y = 10$, $b = h_0 = (12/10^3)^{1/2}$, $E = 10^9/12$, $\nu = 0$, $\rho_0 = 10^3/12$, in order to obtain the same sectional characteristics $EA = 10^6$, $\rho_0 A = 1$, $EJ = 10^3$, as in the examples based on the beam theory. However, our torsional stiffness and rotary inertia following from the shell data are

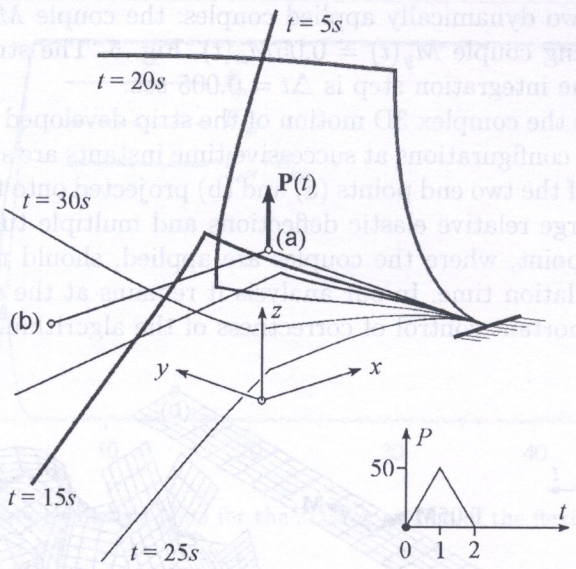

Fig. 7. Right-angle cantilever beam: the applied force data and deformed configurations at five time instants

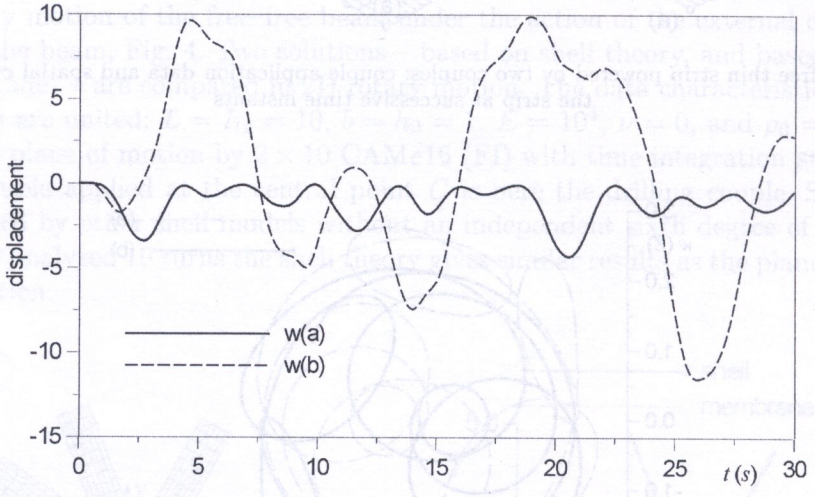

Fig. 8. Time histories of out-of-plane displacements of the points (a) and (b)

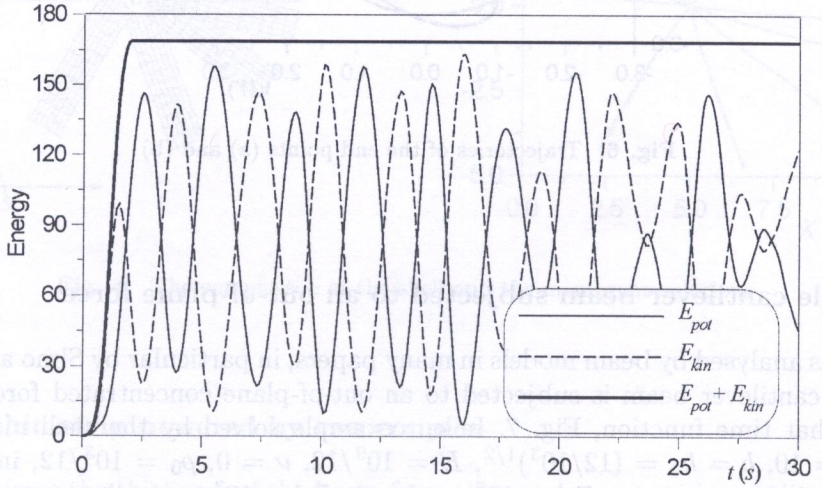

Fig. 9. Energy histories for non-linear vibrations of the right-angle cantilever beam

different from those used in earlier beam papers. Therefore, our results are not comparable to the earlier beam results. The cantilever is discretised into $2 \times 2 \times 10 + 4 = 44$ CAMe9 (FI) elements. After removal of the force the cantilever undergoes finite free vibrations with combined bending and torsion. The time histories of the out-of-plane displacement of the points (a) and (b) are given in Fig. 8. While the values of potential and kinetic energies oscillate in a wide range, Fig. 9, the total energy remains almost constant in time.

6.5. The hemisphere with an 18° hole

The octant panel of the hemisphere with an 18° hole, subjected to the two inward and outward forces applied at the base edges, Fig. 10, with the data $R = 10$, $h_0 = 0.04$, $\alpha = 18°$, $E = 6.825 \times 10^7$, $\nu = 0.3$, $P = \lambda P_{\text{ref}}$, $P_{\text{ref}} = 10$, is often used as a solution convergence test for finite elements. In dynamic analysis of the octant panel, we discuss its large overall motion as in [16]. The applied forces are now ramped from 0 to a value of 50 over 5 sec and ramped back down to 0 in another 5 sec, Fig. 10. The octant panel is discretised by 8×8 CAMe16 (FI) with totally 3750 dof, and the time step $\Delta t = 0.1$ sec is used. Several stages of the deformed octant panel at specified time instants are shown in Fig. 10, while Fig. 11 indicates trajectories of the points (a) and (b) in time, projected onto the X–Y co-ordinate plane. Fig. 12 contains time history plots of the potential, kinetic and total energies.

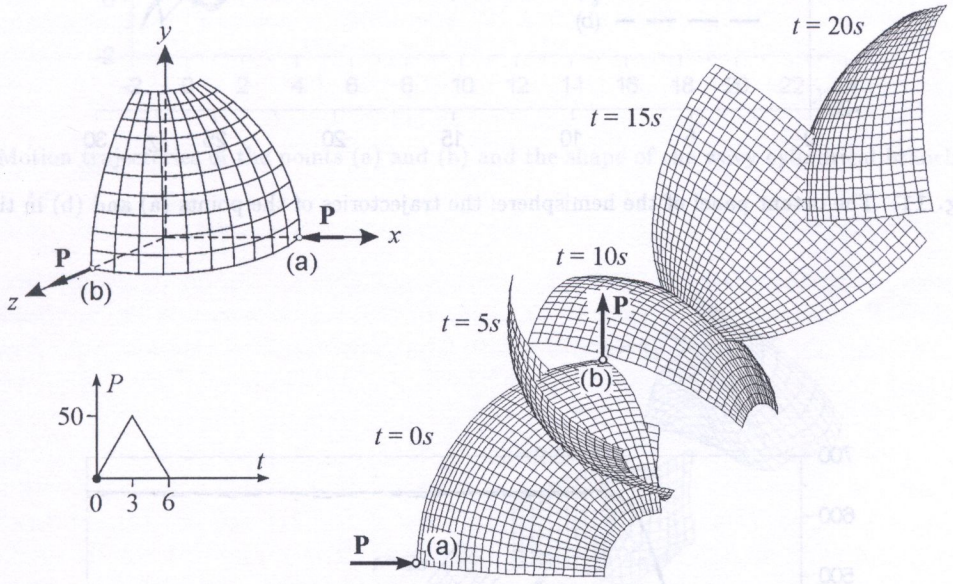

Fig. 10. The octant panel of the hemisphere: the geometry and the applied loading, deformed configurations at specified time instants

6.6. Large motion of a wavy cylindrical branched panel

Consider large motion of a flexible cylindrical panel with change of the curvature sign, reinforced by a plate rib. The shell shape is indicated in Fig. 13, where the data have the following numerical values: $L = 2$, $\alpha = 0.4$, $R = 1$, $H = 0.4$, $h_0 = 0.01$, $E = 10^5$, $\nu = 0.25$, $\rho_0 = 100$, $\rho_0 h_0 = 1$. Two concentrated forces are applied at the points (a) and (b) by the ramp function from 0 to 10 in 1 sec and back down to 0 in another 1 sec. After the 2 sec the shell is free from external loading and moves freely in the space. The panel is discretised by $(5 + 2 + 5) \times 6 = 72$ CAMe9 (FI) with totally 1950 dof and the time step $\Delta t = 0.01$ sec is used. The motion trajectories of the points (a) and (b)

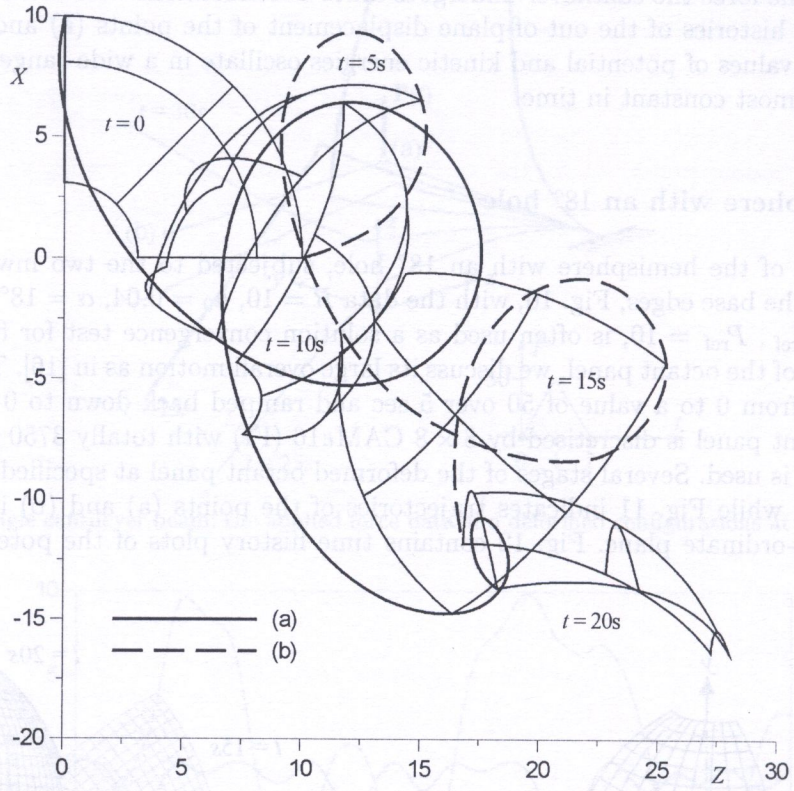

Fig. 11. The octant panel of the hemisphere: the trajectories of the points (a) and (b) in time

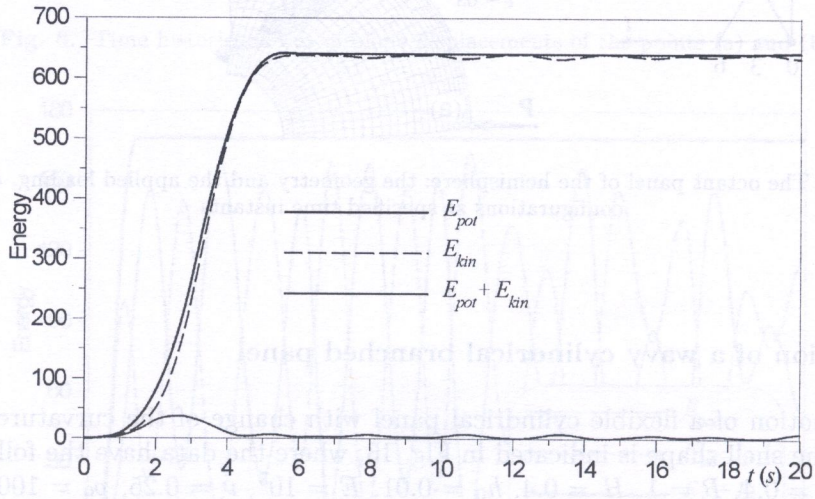

Fig. 12. The octant panel of the hemisphere: time history plots of energies

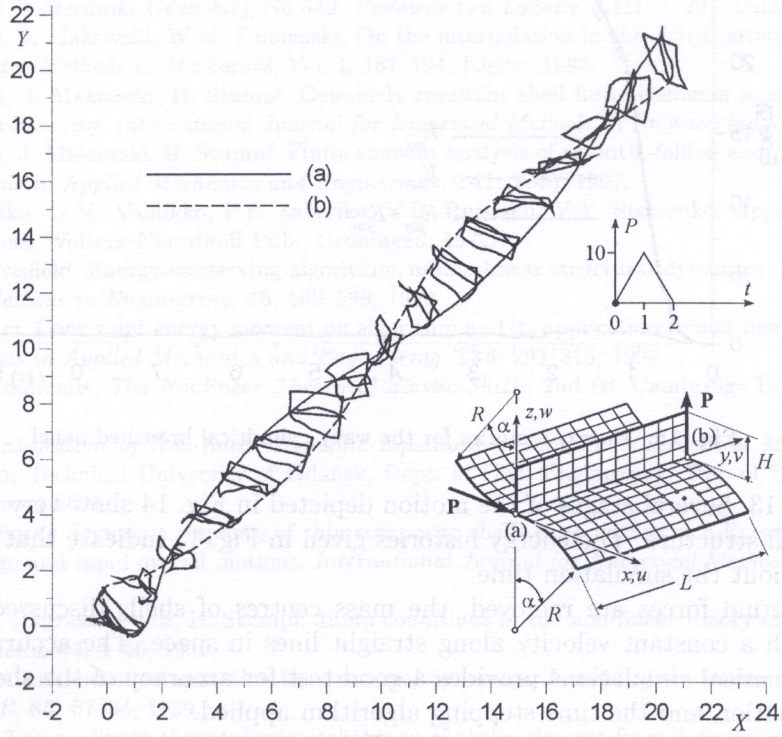

Fig. 13. Motion trajectories of the points (a) and (b) and the shape of the wavy cylindrical branched panel

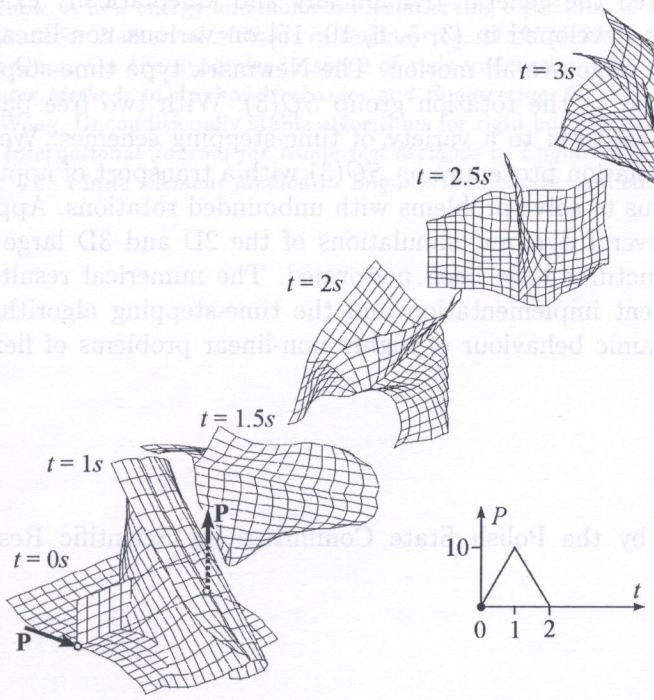

Fig. 14. Deformed configurations in time of the wavy cylindrical branched panel

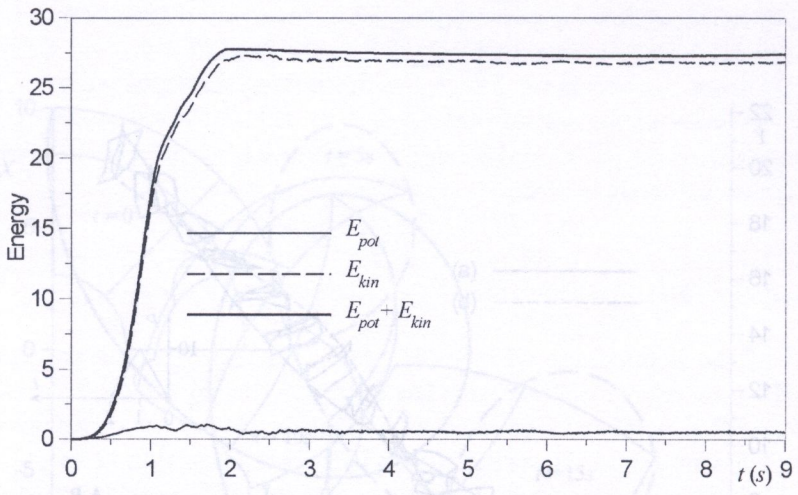

Fig. 15. Energy histories for the wavy cylindrical branched panel

are shown in Fig. 13. Several stages of the motion depicted in Fig. 14 show very large deformations of the flexible shell structure. The energy histories given in Fig. 15 indicate that the total energy is conserved throughout the simulation time.

When the external forces are removed, the mass centres of shells discussed in Examples 6.5 and 6.6 move with a constant velocity along straight lines in space. The accuracy of reproducing the motion in numerical simulations provides a good test for accuracy of the shell theory, its finite element approximation and the time-stepping algorithm applied.

Additional numerical tests were performed by Lubowiecka [11].

7. Conclusions

In this report we have tested the general, dynamically and kinematically exact, six-field theory of branched shell structures developed in [3, 5, 6, 10, 15] on various non-linear problems of shell dynamics involving also the large overall motion. The Newmark type time-stepping algorithm has been developed and extended to the rotation group $SO(3)$. With two free parameters used, our dynamic algorithm can be adjusted to a variety of time-stepping schemes. We have discussed an accurate, indirect C^0 interpolation procedure on $SO(3)$ with a transport of approximation domain. The procedure has allowed us to solve problems with unbounded rotations. Applying the extended time-stepping algorithm, several dynamic simulations of the 2D and 3D large overall motions of various beam and shell structures have been performed. The numerical results confirm that our shell model, its finite element implementation and the time-stepping algorithm can successfully be applied to simulate dynamic behaviour of highly non-linear problems of flexible complex shell structures.

Acknowledgements

This work was supported by the Polish State Committee for Scientific Research under grant No 7 T07A 021 16.

References

[1] B. Brank, L. Briseghella, N. Tonello, F.B. Damjanic. On non-linear dynamics of shells: Implementation of energy-momentum conserving algorithm for a finite rotation shell model. *International Journal for Numerical Methods in Engineering*, **42**: 409–442, 1998.

[2] C. Cardona, M. Geradin. A beam finite element non-linear theory with finite rotations. *International Journal for Numerical Methods in Engineering*, **26**: 2403–2438, 1988.

[3] J. Chróścielewski. The family of C^0 finite elements in the non-linear six-parameter shell theory (in Polish). *Zeszyty Naukowe Politechniki Gdańskiej*, No 540, *Budownictwo Lądowe*, **LIII**: 1–291, Gdańsk, 1996.

[4] J. Chróścielewski, J. Makowski, W.M. Smoleński. On the interpolation in the $SO(3)$ group. In: *Proc. XI Polish Conf. on Computer Methods in Mechanics*, Vol. **I**: 187–194, Kielce, 1993.

[5] J. Chróścielewski, J. Makowski, H. Stumpf. Genuinely resultant shell finite elements accounting for geometric and material non-linearity. *International Journal for Numerical Methods in Engineering*, **35**: 63–94, 1992.

[6] J. Chróścielewski, J. Makowski, H. Stumpf. Finite element analysis of smooth, folded and multi-shell structures. *Computer Methods in Applied Mechanics and Engineering*, **141**: 1–46, 1997.

[7] M.A. Krasnosel'skii, G.M. Vainikko, P.P. Zabreiko, Y.B. Rutitskii, V.Y. Stetsenko. *Approximate Solutions of Operator Equations*. Wolters–Noordhoff Pub., Groningen, 1972.

[8] D. Kuhl, M.A. Crisfield. Energy-conserving algorithms in non-linear structural dynamics. *International Journal for Numerical Methods in Engineering*, **45**: 569–599, 1999.

[9] D. Kuhl, E. Ramm. Constraint energy momentum algorithm and its application to non-linear dynamics of shells. *Computer Methods in Applied Mechanics and Engineering*, **136**: 293–315, 1996.

[10] A. Libai, J.G. Simmonds. *The Nonlinear Theory of Elastic Shells*, 2nd ed. Cambridge University Press, Cambridge, 1998.

[11] I. Lubowiecka. *Integration of Non-linear Dynamic Equations of Motion in Structural Mechanics* (in Polish). PhD Dissertation, Technical University of Gdańsk, Dept. of Civil Engineering, Div. of Structural Mechanics, 142 pages, December 2001.

[12] E. Madenci, A. Barut. Dynamic response of thin composite shells experiencing non-linear elastic deformations coupled with large and rapid overall motions. *International Journal for Numerical Methods in Engineering*, **39**: 2695–2723, 1996.

[13] J. Makowski, W. Pietraszkiewicz, H. Stumpf. Jump conditions in the non-linear theory of thin irregular shells. *Journal of Elasticity*, **54**: 1–26, 1999.

[14] N.N. Newmark. A method of computation for structural dynamics. *Journal of the Engineering Mechanics Division, Proc. ASCE*, **85**: 67–94, 1959.

[15] J.G. Simmonds. The nonlinear thermodynamical theory of shells: descent from 3-dimensions without thickness expansion. In: E.L Axelrad, F.A. Emmerling, eds., *Flexible Shells, Theory and Applications*, 1–11. Springer-Verlag, Berlin, 1984.

[16] J.C. Simo, M.S. Rifai, D.D. Fox. On a stress resultant geometrically exact shell model. Part VI: Conserving algorithms for non-linear dynamics. *International Journal for Numerical Methods in Engineering*, **34**: 117–164, 1992.

[17] J.C. Simo, N. Tarnow. A new energy and momentum conserving algorithm for the non-linear dynamics of shells. *International Journal for Numerical Methods in Engineering*, **37**: 2527–2549, 1994.

[18] J.C. Simo, L. Vu-Quoc. On the dynamics in space of rods undergoing large motions – a geometrically exact approach. *Computer Methods in Applied Mechanics and Engineering*, **66**: 125–161, 1988.

[19] J.C. Simo, K.K. Wong. Unconditionally stable algorithms for rigid body dynamics that exactly preserve energy and momentum. *International Journal for Numerical Methods in Engineering*, **31**: 19–52, 1991.

[20] O.C. Zienkiewicz. *The Finite Element Method in Engineering Science*, 2nd ed. McGraw–Hill, London, 1971.